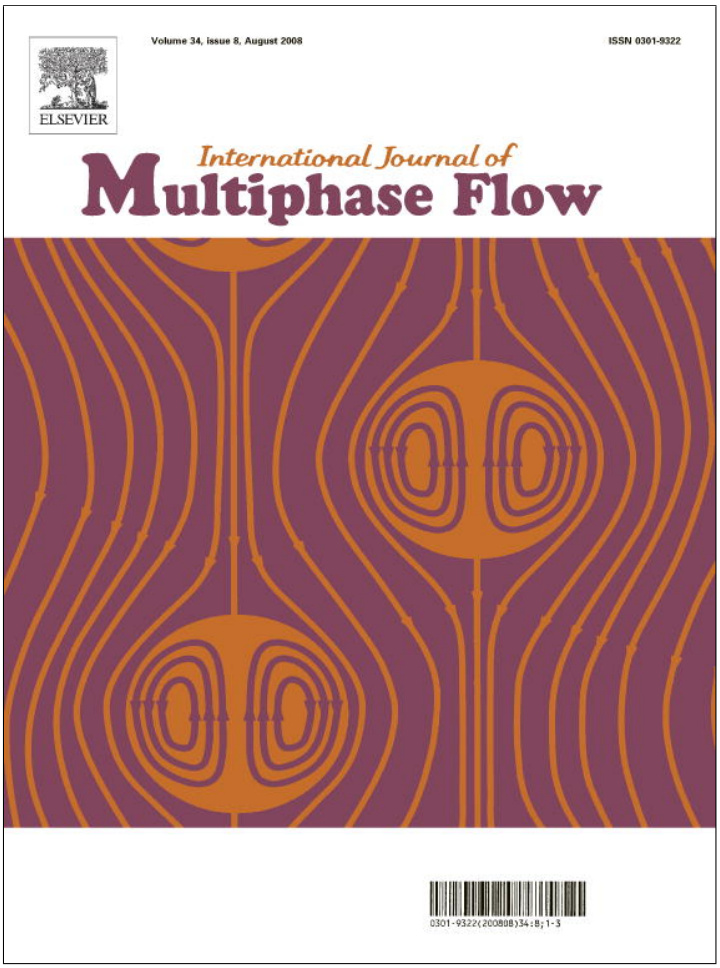

Available online at www.sciencedirect.com
ScienceDirect
International Journal of Multiphase Flow 34 (2008) 734–747
International Journal of Multiphase Flow
www.elsevier.com/locate/ijmulflow

Falling film flow along steep two-dimensional topography: The effect of inertia

V. Bontozoglou *, K. Serifi

Department of Mechanical and Industrial Engineering, University of Thessaly, Pedion Areos, GR-38334 Volos, Greece

Received 5 July 2007; received in revised form 21 November 2007

Abstract

Steady film flow along a vertical wall with isolated step changes is studied numerically for Reynolds numbers $Re \sim O(10^{-3}–10^{2})$ and capillary numbers $Ca \sim O(10^{-2}–10^{1})$. The lengthscale of free surface capillary features upstream of a step-in or step-out decreases uniformly with Re and switches from a $-1/3$ to a $-1/2$ power-law dependence on Ca. The height of the capillary features first grows with Re, but eventually diminishes when inertia forces overpower capillary forces. Simultaneously, the key dynamics move from upstream to downstream of the step, and switch from capillary arrest to inertial re-directioning of the falling liquid. The latter mechanism involves a low-pressure region originating from the edge of the step. At a step-out, a new free surface feature appears with increasing Re, which is caused by liquid overshoot in the horizontal direction and is restrained initially by capillary and subsequently by inertial forces. Simple scaling arguments are shown to predict many of the above characteristics.

Keywords: Falling film; Topography; Step; Inertia; Capillary

1. Introduction

Liquid film flows occur in a variety of scales ranging from geophysical to biological, and are of central importance in many industrial processes. The surface on which the film moves is frequently irregular, either intentionally or accidentally. Indicative examples are provided by the corrugated surfaces used for heat/mass transfer intensification in process equipment (Webb, 1994; Valluri et al., 2005), and by the various coating and film deposition processes employed in the manufacture of electronic components and digital storage devices (Stillwagon and Larson, 1990). In the latter applications, it is rotational motion (e.g. as in spin coating) rather than gravity that drives the fluid film. For this reason, the study of a film whose mean direction of flow coincides with the direction of the driving force is of special interest.

An interesting topic of investigation is the response of the liquid film to topographic changes, such as step-in and/or step-out. Most of the relevant studies have invoked the lubrication approximation in the limit of Stokes flow (Stillwagon and Larson, 1990; Prichard et al., 1992; Kalliadasis et al., 2000; Aksel, 2000; Kalliadasis and Homsy, 2001; Decre and Baret, 2003; Gaskell et al., 2004). Important results are the confirmation of the accuracy of the lubrication approximation even outside its formal range of validity, and the identification of robust capillary features at the upstream side of steep topographic changes. More specifically, a ridge is seen to form before a step-in and a depression before a step-out. An early numerical investigation of this problem, again in the Stokes limit, was performed by Pozrikidis (1988). More relevant to the present study is the recent numerical investigation by Mazouchi and Homsy (2001), which provides a complete interpretation of the dynamical role of the capillary ridge.

The importance of including inertia effects in film flows has been discussed repeatedly (see for example Oron et al.,

* Corresponding author. Tel.: +30 24210 74069; fax: +30 24210 74085.
E-mail address: bont@mie.uth.gr (V. Bontozoglou).

0301-9322/$ - see front matter © 2008 Elsevier Ltd. All rights reserved.
doi:10.1016/j.ijmultiphaseflow.2008.01.006

1997). However, most of the available results for an uneven wall refer either to constant curvature (Kalliadasis and Chang, 1994; Kliakhandler et al., 2001; Noakes et al., 2006) or to slowly varying curvature (Ruschak and Weinstein, 2003; Roberts and Li, 2006). Khayat et al. (2004) reported on the transient effects of inertia in axisymmetric film flow over smooth step-ins and step-outs. Gaskell et al. (2004) computed some steady, finite-*Re* flows along two-dimensional orthogonal cavities, in a study mainly focused on localized (three-dimensional) topography in the lubrication limit.

It is evident from the above that the available information on the finite-*Re* behavior of films flowing over steep topography is limited and fragmentary. Thus, in the present paper we consider a vertical film flowing along a wall with isolated steps of size up to the order of the film thickness. Steady state is assumed, and the Navier–Stokes equations of motion are solved numerically by a finite-element technique.

We note right away that our investigation leaves open the question of stability of the computed steady solutions. However, – apart from their use as a starting point for stability analysis – steady solutions of the present problem are argued to be of physical significance even when unstable. This happens because film flows are convectively unstable. Thus, the base flow is only temporarily disrupted by traveling disturbances and is re-established as soon as the disturbances move downstream.

The paper outline is as follows: The problem setup and the computational procedure are described in Section 2. Section 3 presents the results, which consist of numerical predictions of the free surface characteristics and of their parametric variation with *Re* and *Ca*. In Section 4, we try to interpret these results by invoking simple scaling arguments and by investigating the structure of the flow. Finally, Section 5 reviews the main conclusions.

2. Problem setup and computational procedure

We consider steady, two-dimensional free surface flow of a thin liquid film down a vertical wall with isolated steps of depth D (Fig. 1a). The liquid has density, viscosity and surface tension ρ, μ and σ respectively, and the flow is uniform in the transverse direction with volumetric flow rate per unit span Q. Coordinates x and y originate from the upper flat wall and correspond respectively to the streamwise (vertical) and normal (horizontal) direction. The location of the free surface is denoted by $y = h_0(x)$. The characteristic scales are based on the classical Nusselt solution for flow along a flat wall, i.e. a film of uniform thickness $H = (3\nu Q/g)^{1/3}$ and parabolic velocity profile $u_0(y) = g(2Hy - y^2)/2\nu$ with mean velocity $U = Q/H = gH^2/3\nu$, where $\nu = \mu/\rho$.

A complete description of the flow is provided by the continuity and the steady form of the Navier–Stokes equation, together with the appropriate set of wall and free surface boundary conditions. Scaling lengths with H, velocities with U and pressure with ρU^2 results in the following dimensionless equations:

$$\nabla \cdot \mathbf{u} = 0, \tag{1}$$

$$(\mathbf{u} \cdot \nabla)\mathbf{u} = -\nabla p + \frac{1}{Re}\nabla^2 \mathbf{u} + \frac{3}{Re}\mathbf{g}. \tag{2}$$

Here $\mathbf{u} = (u, v)$ is the dimensionless velocity vector, with u and v its components in the x- and y-direction, respectively, p is the dimensionless pressure and $\mathbf{g}$ is the unit vector in the direction of gravity. *Re* is the Reynolds number, defined as $Re = Q/\nu = UH/\nu$.

We further apply the no-slip and no-penetration boundary condition for the velocity along the wall,

$$u = v = 0, \tag{3}$$

and the kinematic condition and balance of forces along the free surface

$$u\frac{\mathrm{d}h}{\mathrm{d}x} = v, \tag{4}$$

$$\mathbf{n} \cdot \mathbf{T} = \frac{3}{Ca\,Re} 2H_c \mathbf{n}. \tag{5}$$

Here, h is the dimensionless free surface location, $\mathbf{n}$ is the unit vector normal to the free surface, $2H_c = (\mathrm{d}^2h/\mathrm{d}x^2)/$

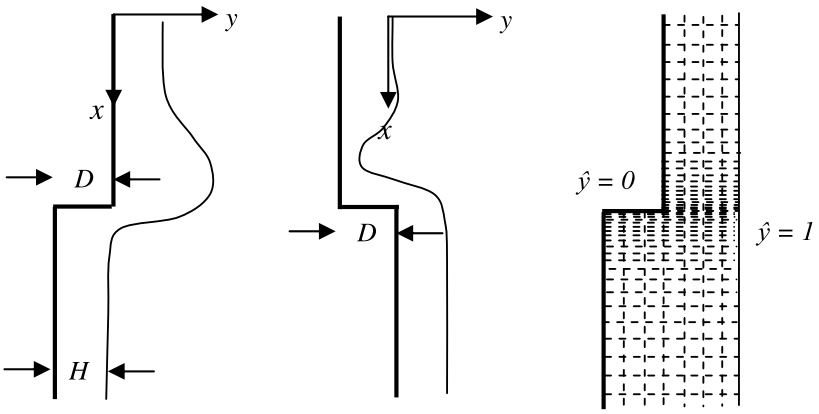

Fig. 1. (a) The physical flow domain about a step-in and a step-out and (b) the computational domain of a step-in with a sketch of the finite-element grid.

$[1+(\mathrm{d}h/\mathrm{d}x)^2]^{3/2}$ is the free surface curvature, $Ca = 3\mu U/\sigma = \rho g H^2/\sigma$ is the capillary number and

$$\mathbf{T} = -p\mathbf{I} + \frac{1}{Re}[\nabla\mathbf{u} + (\nabla\mathbf{u})^{\mathrm{T}}] \tag{6}$$

is the dimensionless stress tensor of the fluid, with $\mathbf{I}$ the identity matrix. Finally, the computational inlet and outlet are taken far enough from the cavity that the flow locally corresponds to the undisturbed Nusselt solution.

According to the above, the problem is described by the two dimensionless numbers Re and Ca, which express respectively the ratios of inertia over viscous forces and of viscous over capillary forces. Alternatively, Ca may be substituted by the Weber number

$$We = \frac{Re\,Ca}{3} = \frac{\rho H U^2}{\sigma}, \tag{7}$$

which expresses the ratio of inertia over capillary forces. As expected, the Weber number is more relevant than the capillary number in the limit of high Re. The depth of the step introduces an additional length ratio

$$\delta = \frac{D}{H}. \tag{8}$$

The steps presently considered have depths ranging from small up to comparable with the film thickness, with emphasis placed on the latter. Steps significantly deeper than the film are expected to facilitate detachment of the liquid from the wall, a phenomenon beyond the scope of the present work.

The above set of equations and boundary conditions is solved by a standard Galerkin finite-element method. The primary unknowns of the flow, which are the velocities u and v, the pressure p and the location of the free surface h, are expanded respectively in terms of bi-quadratic, bilinear and quadratic basis functions. The governing equations, weighted integrally with the basis functions, result in the continuity, momentum, and kinematic residuals, which are evaluated numerically using nine-point Gaussian integration, and are solved for the unknown nodal values by a Newton–Raphson iterative scheme. The computational methodology has been described in detail elsewhere (Malamataris et al., 2002).

Implementation details specific to the present application are demonstrated in Fig. 1b, which shows the mesh for a step-in. The computational domain is taken equal to 80 dimensionless lengths and the face of the step is always positioned at the middle ($\hat{x} = 40$). Finite-element nodes are distributed in the y-direction so that their number increases when passing from the out-hanging to the retracted side of the wall. The increase is roughly proportional to the ratio of step depth to film thickness, so that the y-separation of consecutive nodes does not change drastically and the elements are only mildly distorted. Thus, the y-locations before and after a step-in are given respectively by the following relations:

$$y = \hat{y}h(x) \quad \text{and} \quad y = \hat{y}[\delta + h(x)] - \delta, \tag{9}$$

where $\hat{y}$ takes values always in the interval $[0,1]$ but with different densities before and after the corner. On the face of the step, the additional nodes are held at fixed positions from the bottom to the edge, so that the edge always corresponds to a node.

With respect to the grid distribution in the x-direction, node clustering around the edge has been used to improve the accuracy in the vicinity of the step. To that end, we have applied the following algebraic rule:

$$x = w\left\{\alpha\xi + (1-\alpha)\left[1 - \frac{\tanh[\beta(1-\xi)]}{\tanh\beta}\right]\right\}, \tag{10}$$

where w is the distance from the inlet to the step, ξ is equidistributed in $[0,1]$ and α, β are stretching parameters. A typical computational mesh of the present study uses $\alpha = 1.9, \beta = 2.0$, and involves 300 elements in the streamwise direction, 10 elements above the overhanging wall and 20 elements above the retracted wall. Finer grid in the y-direction has been used to discretize deeper steps and grid independence has been tested by doubling the number of elements in both directions.

3. Results

3.1. The limit of creeping flow

We initially reproduce the results of Mazouchi and Homsy (2001) for Stokes flow along an extensive one-dimensional cavity (i.e. a step-in and a step-out separated by 40 dimensionless length units). Fig. 2 shows the deformation of the free surface as a function of Ca for $\delta = 1$ and $Re = 0.001$, and very good agreement is confirmed. As already noted, the capillary features at the step-in are stronger than at the step-out, and they are also dynamically more significant. To this end, we recall Mazouchi and Homsy's interpretation of the role of the inlet ridge, as providing the pressure differential for pushing the liquid inside the cavity, i.e. in the direction normal to the gravity force that drives the mean motion.

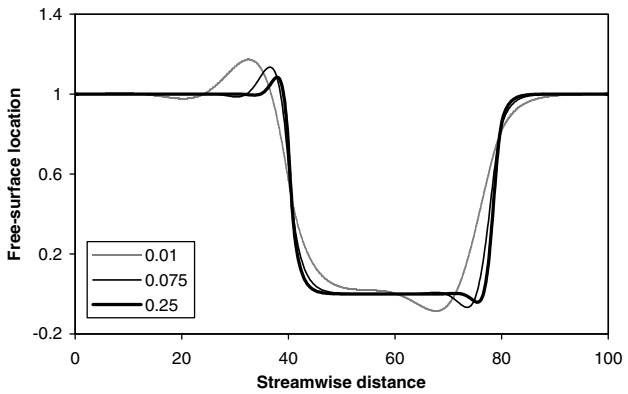

Fig. 2. The location of the free surface along a cavity of dimensionless length 40 and depth $\delta = 1$, for $Re = 0.001$ and $Ca = 0.01$, 0.075 and 0.25.

The balance of gravity and capillary forces determines the streamwise scale of the free surface deformations (Kalliadasis et al., 2000) as

$$l = \frac{L}{H} \approx Ca^{-1/3}. \tag{11}$$

This scaling is valid both before the step-in and the step-out. According to Eq. (11), the capillary features grow in length with increasing surface tension. Mazouchi and Homsy also showed that at the opposite end of decreasing surface tension the deformation diminishes exponentially so as to keep providing the driving force at the correct scale.

The height of the capillary features (i.e. the positive or negative deviation from the flat free surface, $h_{cap} - 1$, where h_{cap} is the film height at the ridge or depression) is expected to depend on the depth of the step. Predictions for creeping flow ($Re = 0.001$) are provided in Fig. 3. In the limit of an infinitesimal step, the height of the ridge before the step-in and the height of the depression before the step-out coincide and are roughly equal to 10% of the depth of the step. This symmetry is broken in opposite directions with increasing step size: The ridge grows faster than the step and the depression slower, with the deviation becoming quantitatively significant when $\delta = O(1)$. However, because the rate of change with δ is roughly uniform, there appears to exist no strictly linear region where $(h_{cap} - 1)/\delta \sim$ const. In this sense, the criterion $\delta < 0.5$ proposed by Decre and Baret (2003) must be considered more a convenient approximation than a rigorous limit.

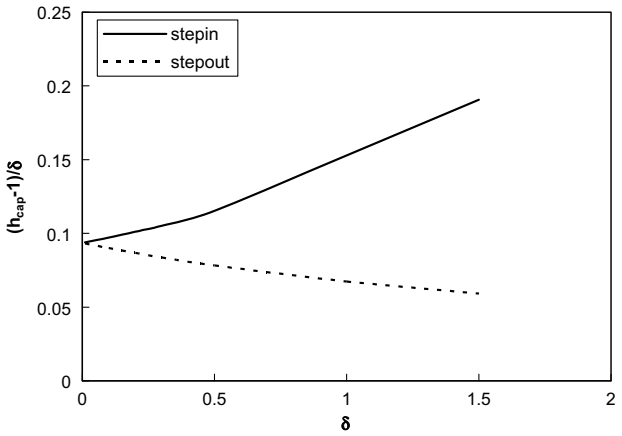

Fig. 3. The height of the capillary features upstream of a step-in and a step-out in the limit of creeping flow ($Re = 0.001$), as a function of the depth of the step. Note that, in the figure, the height is normalized with the step depth.

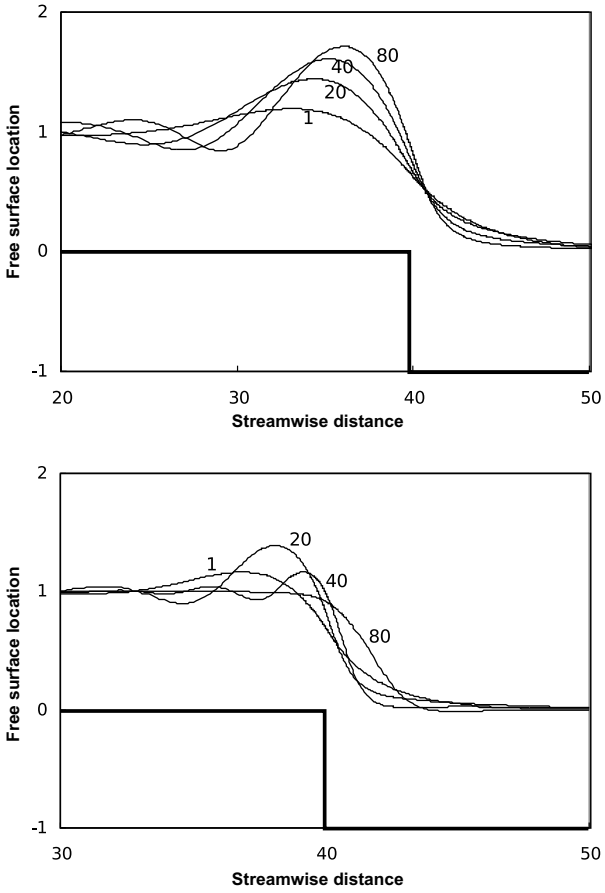

Fig. 4. The free surface profiles in the vicinity of a step-in with $\delta = 1$, for $Re = 1$, 20, 40, 80 and (a) $Ca = 0.01$, (b) $Ca = 0.075$.

3.2. The effect of inertia at a step-in

The combined effects of inertia and capillarity on the free surface characteristics are introduced in Fig. 4a and b, which presents free surface profiles as a function of Re for a step-in with dimensionless depth $\delta = 1$ and capillary numbers $Ca = 0.01$ and 0.075, respectively. It is readily observed that the streamwise lengthscale of the capillary features uniformly decreases with both Re and Ca. Also, with increasing Re the free surface becomes wavier and the ridge is gradually transformed into a series of damped stationary capillary waves. The shortening of the capillary length with increasing inertia is accompanied by a gradual displacement of the ridge extremum towards the topographic discontinuity.

The height of the capillary ridge varies inversely with Ca, i.e. strong surface tension results in more pronounced features. However, the dependence on inertia is strickingly non-monotonic. With increasing Re, the capillary ridge initially grows in height, reaching a maximum that is significantly higher than the creeping flow value, but then decreases and eventually disappears altogether. This evolution is postponed to higher Re with decreasing Ca. Thus, the disappearance of the capillary features is manifested in Fig. 4b, whereas it has not yet occurred for the Re range depicted in Fig. 4a.

The parametric variation of the characteristics of the capillary ridge is shown in detail in Fig. 5a–c. The dependence of the ridge height on Re and Ca is depicted in Fig. 5a for $\delta = 1$. With decreasing Ca, the maximum height becomes stronger, occurs at higher Re and is accompanied by a wider plateau. The disappearance of the ridge with

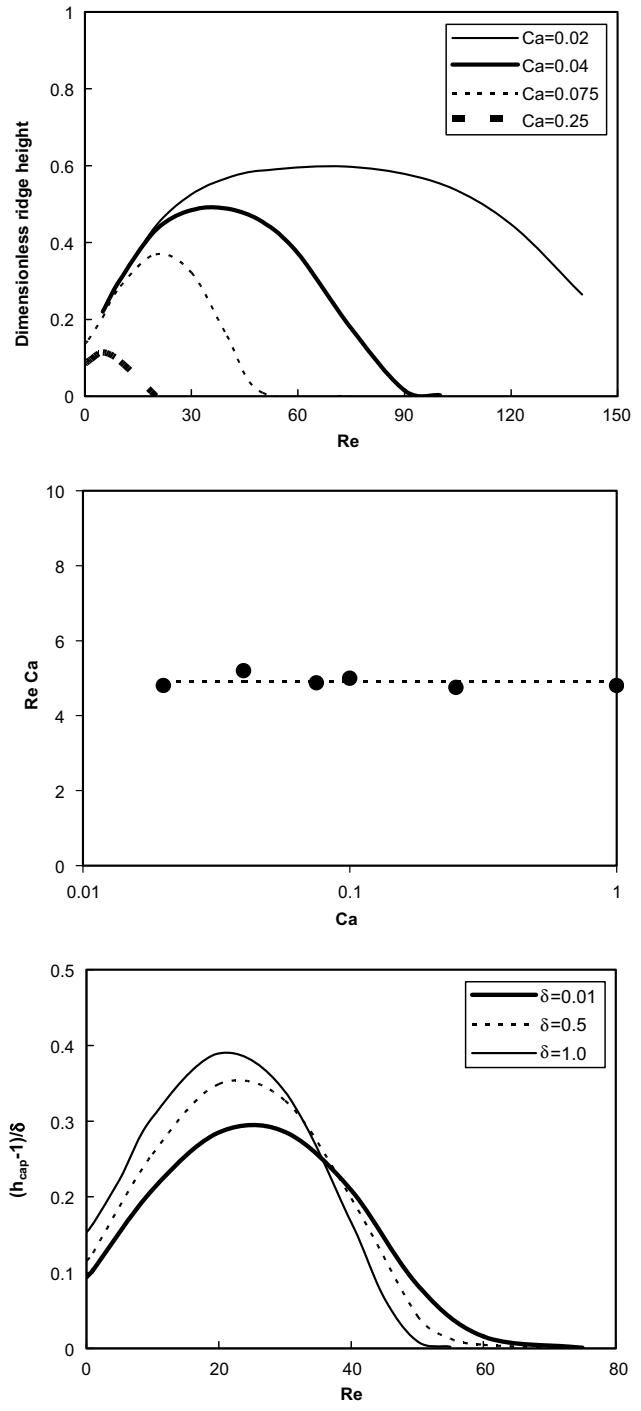

Fig. 5. Parametric variation of the height of the capillary ridge upstream of a step-in: (a) The ridge height as a function of Re for various Ca. (b) The conditions where the ridge disappears. Points are numerical data and the line is the function $Re\,Ca = 4.9$. (c) The ridge height, normalized with δ, as a function of Re for dimensionless step depths $\delta = 0.1$, 0.5, 1.

increasing inertia occurs at a Re inversely proportional to Ca. This trend is confirmed by Fig. 5b, where points are numerical data indicating values of the product $Re\,Ca$ where the ridge ceases to exist for $\delta = 1$ and the line corresponds to $Re\,Ca = 4.9$. The disappearance of the ridge at a constant value of the Weber number ($We = Re\,Ca/3 = 1.63$) is evidently interpreted as a result of the dominance of inertia over capillary forces.

The effect of the dimensionless depth, δ, is shown in Fig. 5c, where the ridge height divided by δ is plotted as a function of Re for $Ca = 0.075$ and $\delta = 0.01$, 0.5 and 1.0. Deepening of the step-in in this range leads to a significantly stronger effect on the free surface and displaces both the maximum and the disappearance of the ridge to lower Re. As a consequence of the latter, the numerical value of Weber number that corresponds to the disappearance of the ridge is not constant but varies with the dimensionless depth of the step. Some indicative values of We as a function of δ are given in Table 1.

The characteristics of the free surface may interact with the local structure of the flow imposed by the steep topographic change. In particular, the flow along a step-in will undergo at finite Re inertial separation, and the effect of the resulting eddy is expected to be significant, in particular at $\delta \sim O(1)$. A representative evolution of the separation eddy with increasing Re is shown in Fig. 6 for $Ca = 0.075$ and $\delta = 1$. (Note that the scale is stretched in the y-direction, so that both the separation region and the free surface features are accommodated.) It is observed that the eddy initially grows, then remains roughly constant in size for a significant range of Re (10–40) and finally continues to grow after the disappearance of the capillary ridge. Also, with increasing Re the free surface over the step tends progressively to align with the separatrix, and eventually becomes parallel to it after the disappearance of the ridge.

Two additional flow details, which occur in a limited range of the parameter space, are shown in Fig. 7. Fig. 7a documents that, at very small Re($Re = 1$, $Ca = 0.075$), the separation along a deep step-in may be restricted to the edge of the step. The flow re-attaches further along the face of the step and separates again in the vicinity of the corner. Fig. 7b refers to conditions leading to a high capillary ridge ($Re = 100$, $Ca = 0.02$) and shows that the combination of intense capillary wrinkling and increased inertia may result in an additional separation region below the ridge and before the edge of the step.

3.3. The effect of inertia at a step-out

The combined effects of inertia and capillarity on the free surface characteristics are introduced by Fig. 8, which presents free surface profiles as a function of Re for a step-

Table 1
The We number corresponding to the disappearance of upstream capillary waves at a step-in, as a function of dimensionless step depth, δ

δ	We
0.01	2.02
0.1	1.99
0.2	1.94
0.5	1.80
1.0	1.63
1.5	1.61

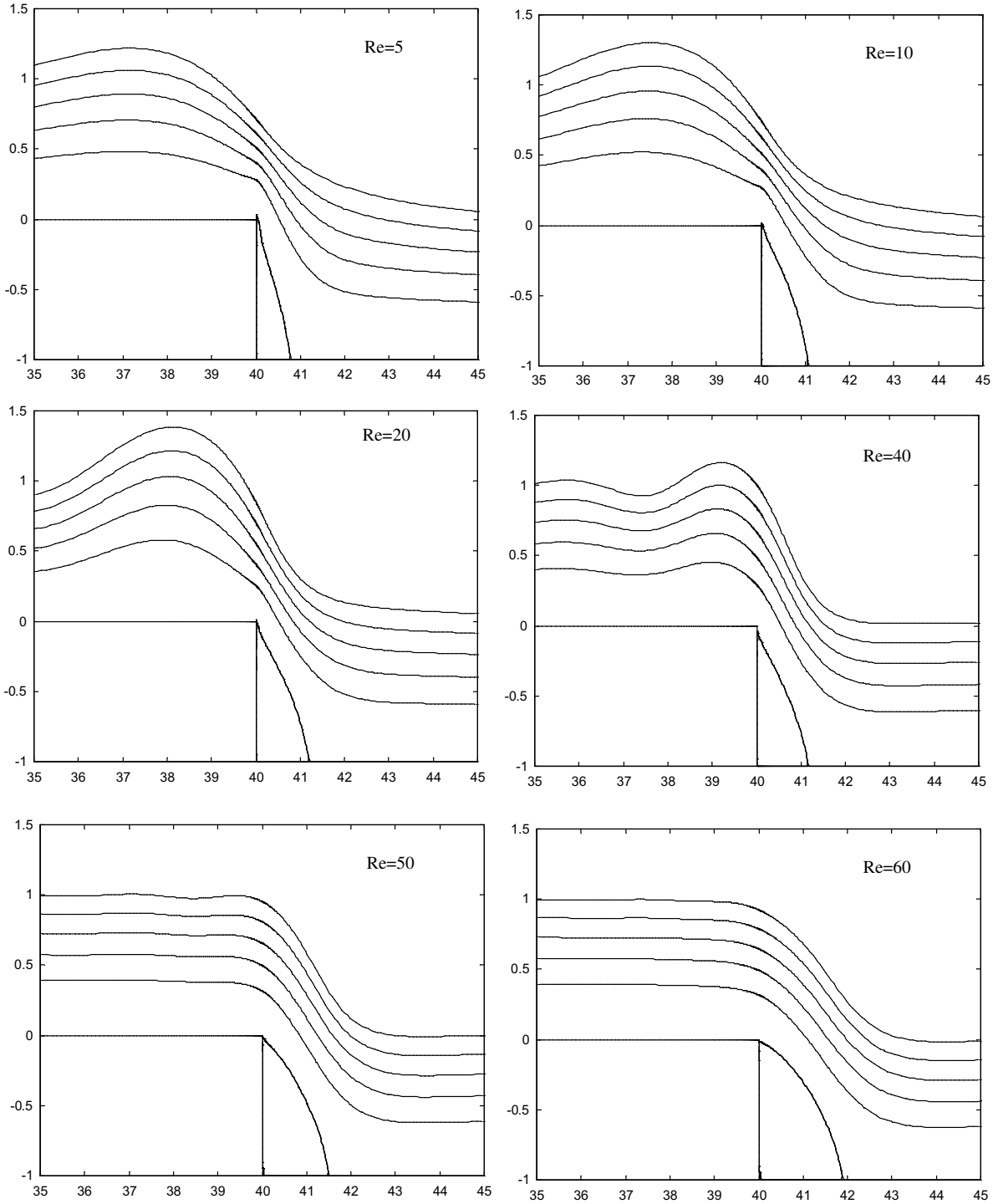

Fig. 6. The evolution with increasing *Re* of the flow field around a step-in with $\delta = 1.0$, for $Ca = 0.075$.

out with dimensionless depth $\delta = 1.5$ and capillary number $Ca = 0.075$. It is observed that – similarly to the behavior at a step-in – the capillary features upstream of the step become more oscillatory and their streamwise length uniformly decreases with *Re*. Also, with increasing *Re* the depression initially grows in height but then declines and eventually disappears.

A new characteristic of the flow at high *Re* that is evident in Fig. 8 is the appearance of a ridge after the step-out, which is evidently caused by an overshoot of the liquid film as it is deflected in the horizontal direction by the step. We call this feature the inertial ridge. The parametric variation of the characteristics of the inertial ridge is shown in detail in Fig. 9a and b. The dependence of the ridge height on *Re* is depicted in Fig. 9a for $\delta = 1.5$ and $Ca = 0.02$, 0.04, 0.075 and 0.25. Two different types of behavior are noted with increasing *Re*: Initially the height of the ridge varies strongly with *Ca*, but then the curves for all *Ca* nearly con-

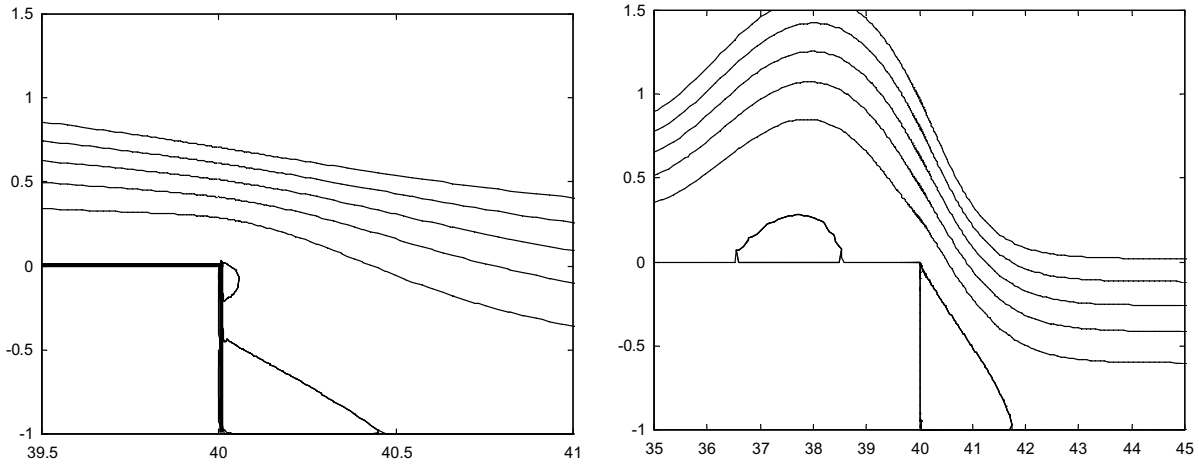

Fig. 7. (a) The onset of separation along the edge of a step-in at $Re = 1$, $Ca = 0.075$, and (b) the formation of a separation eddy below an intense capillary ridge at $Re = 100$, $Ca = 0.02$.

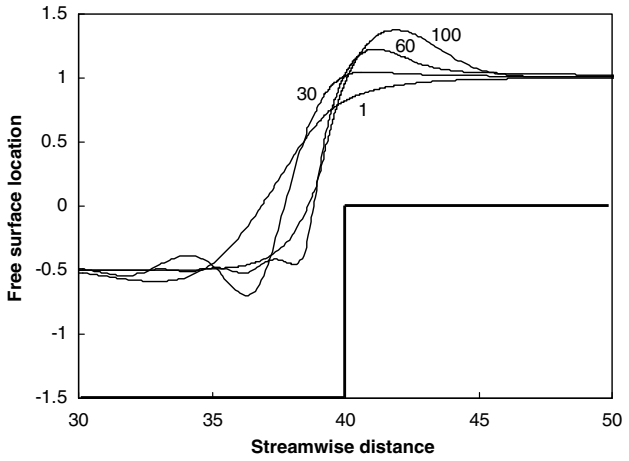

Fig. 8. The free surface profiles in the vicinity of a step-out with $\delta = 1.5$, for $Ca = 0.075$ and $Re = 1$, 30, 60, 100.

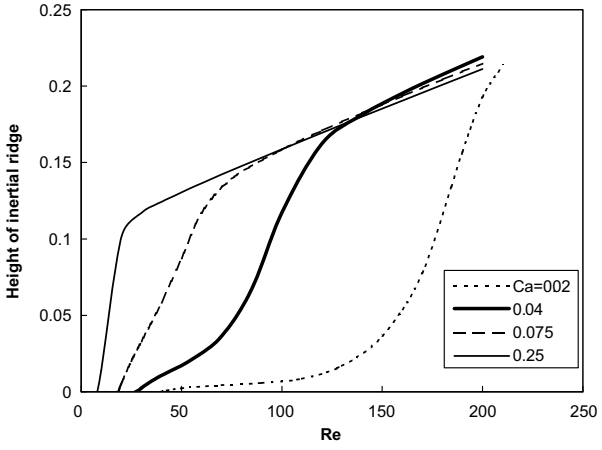

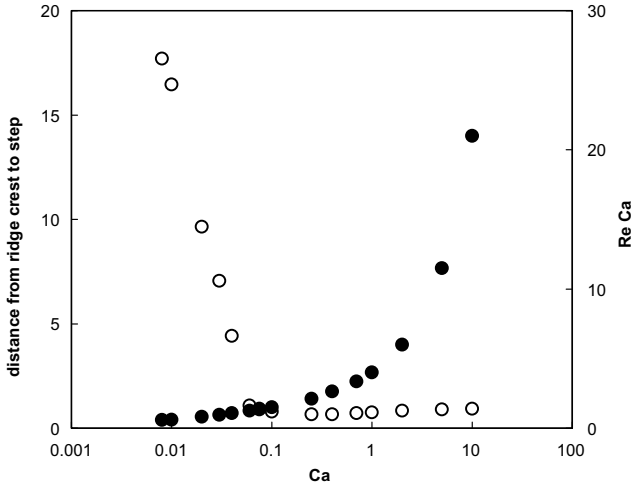

Fig. 9. Parametric variation of the inertial ridge at a step-out with $\delta = 1.5$: (a) The ridge height as a function of Re for various Ca. (b) The conditions ($Re\,Ca$) where the ridge appears (dark circles – right axis), and the distance from the edge of the step to the crest of the ridge (open circles – left axis) as a function of Ca.

verge. This trend indicates that surface tension, which restrains the ridge at low Re, is replaced by an inertial mechanism at high Re. Therefore, the asymptote represents the limit of negligible capillary forces, as is indeed confirmed by noting that the curve for each Ca depicted joins the asymptote at a Re inversely proportional to Ca ($We \sim 1.9$).

In accord with the significance of capillary forces at low/intermediate Re, the inertial ridge appears at a Re that varies inversely with Ca. However, the transition does not occur at a constant We. Representative numerical data are shown in Fig. 9b for $\delta = 1.5$ (closed circles – right axis), and indicate that the values of the product $Re\,Ca$ span more than an order of magnitude. Also depicted in the figure is the distance from the crest of the ridge to the edge of the step (open circles – left axis). It is observed that the emerging deformation is very elongated at low Ca, but attains a size of the order of the film thickness at high Ca. A scaling analysis will be presented in the discussion section that interprets this behavior.

The effect of the dimensionless depth, δ, on the size of the ridge is shown in Fig. 10, where the ridge height divided

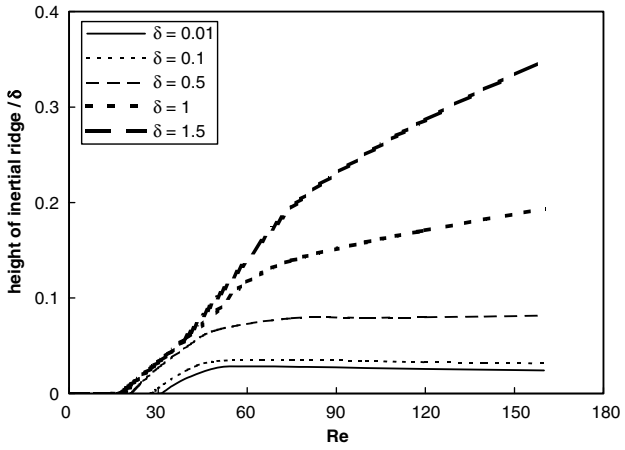

Fig. 10. The ridge height, divided by δ, as a function of Re for dimensionless step depths $\delta = 0.01$, 0.1, 0.5, 1.0 and 1.5. The near-coincidence of the $\delta = 0.01$ and 0.1 curves confirms the initial linear dependence of ridge height on δ.

by δ is plotted as a function of Re for $Ca = 0.075$ and $\delta = 0.01$, 0.1, 0.5, 1.0 and 1.5. We observe that for $\delta \ll 1$ the data collapse to one curve, i.e. in the linear limit the ridge scales with the depth of the step. Increasing δ, results in an impressive growth of the protrusion with Re, and in a shift of its onset to lower Re. For $\delta \sim O(1)$, the onset asymptotes to a roughly constant Re, but the ridge height at high Re keeps growing with δ. This behavior may be understood by considering that the horizontal part of the step serves as a launching pad for the liquid to be ejected in the y-direction. Thus, the deeper the step the more complete the transformation of the x-momentum into y-momentum.

As with the step-in, the characteristics of the free surface along a step-out may interact with the local structure of the flow imposed by the steep topographic change. A representative evolution of the structure of the flow with increasing inertia is shown in Fig. 11 for Ca = 0.075 and $\delta = 1.5$, and demonstrates the existence of two separation regions. The one at the foot of the step is affected by the abruptness in change of flow direction. It initially grows with Re, then shrinks as the capillary waves are pushed towards the step and eventually grows again after the waves disappear.

At high Re, an additional separation region appears below the inertial ridge; it originates at the edge of the step, is elongated in the streamwise direction and grows constantly with Re. Thus, it is noted that – unlike the situation at the step-in – separation at the edge of the step-out necessitates a significant magnitude of inertia. The difference between the two is explained by the role of gravity, which in the former case promotes detachment of the film from the wall, whereas in the latter assists the film to stay attached.

4. Discussion

In the previous section, the main characteristics of steady, vertical film flow along isolated step-ins and step-outs were numerically documented. In the discussion that follows, we will try to understand this phenomenology by invoking simple scaling arguments and by examining further the structure of the flow field.

4.1. The capillary lengthscale

The scaling arguments of Kalliadasis et al. (2000) and Mazouchi and Homsy (2001) may be extended to finite inertia in order to predict the streamwise length of the capillary features. More specifically, at small to intermediate Re the capillary pressure at the step-in is still the main force driving the fluid horizontally (i.e. normal to the direction of gravity), but it must now be sufficient to overcome the combined effect of the gravitational force and film inertia. The same force balance applies upstream of the step-out, where the capillary depression appears as a reaction to the weight of the film and to the change in flow direction.

Denoting by $l = L/H$ the dimensionless streamwise scale of the capillary features before the step, and taking their height to be at most comparable to the film thickness, we may write the following order-of-magnitude estimate of the streamwise momentum balance:

$$\rho g + \frac{\rho U^2}{L} \approx \sigma \frac{H}{L^3} \Rightarrow l^3 + \left(\frac{Re}{3}\right) l^2 \approx \frac{1}{Ca}. \tag{12}$$

Here, the pressure gradient has been approximated as $\partial p/\partial x \approx \sigma \partial^3 h/\partial x^3$ according to the capillary contribution of the free surface boundary condition. The influence of viscous forces that appears to be neglected in Eq. (12) is in fact hidden in the definition of the velocity scale, U, which results from a balance of the undisturbed viscous and gravity forces. Thus, the term "ρg" on the l.h.s. of Eq. (12) actually represents the local imbalance between gravity and viscous forces.

Two limits are identified in Eq. (12). Neglecting inertia we recover the Stokes scaling, Eq. (11). In the opposite limit of dominant inertia over gravity, we take the high-Re limit

$$l \approx Re^{-1/2} Ca^{-1/2} \approx We^{-1/2}. \tag{13}$$

The sole dependence of the capillary lengthscale on We number (i.e. the ratio of inertia to capillary forces) indicates that viscous forces have no additional dynamic role apart from the definition of the velocity scale, U. A criterion of transition from the capillary-gravity to the capillary-inertia regime is provided by equating the two terms on the l.h.s. of Eq. (12) and substituting back the resulting value $l = Re/3$. Thus, we find for the transition Reynolds number, Re_t,

$$Re_t = \frac{3}{(2Ca)^{1/3}}. \tag{14}$$

The above scaling estimates are now checked by comparison with numerical results. We have tried more than one way to define the streamwise length scale, l, and have

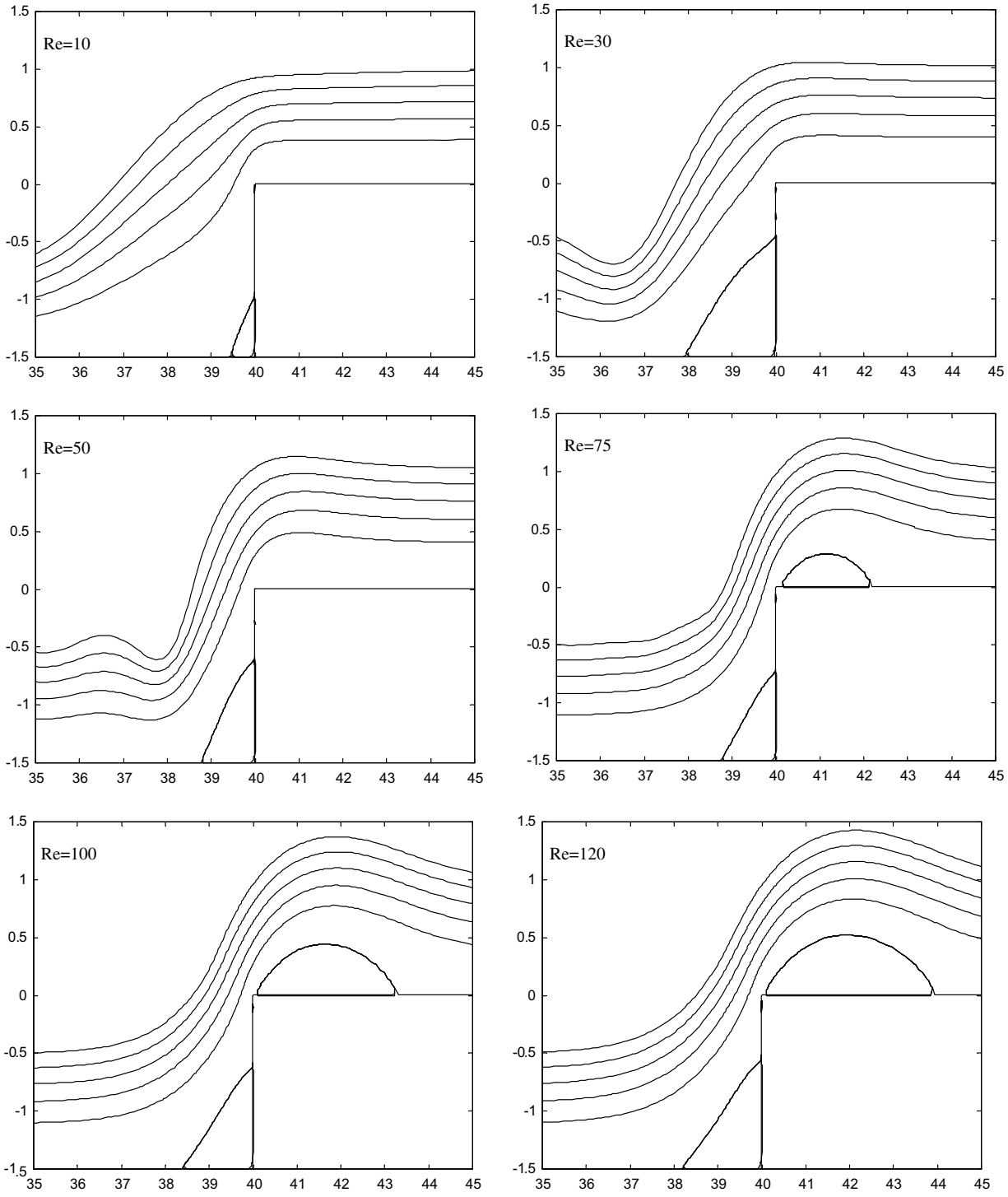

Fig. 11. The evolution with increasing Re of the flow field around a step-out with $\delta = 1.5$, for $Ca = 0.075$.

found that the trends to be discussed next are insensitive to the specific choice. Eventually, we adopted the definition shown in Fig. 12, which sets the lengthscale equal to the section, AB, marked on the $y = H$ horizontal line by the two tangents to the main ridge at the locations of maximum absolute slope. We also confirmed that the ridge before a step-in and the depression before a step-out scale in exactly the same way, and we present data only for the former.

The values of l calculated according to the above procedure are plotted in Fig. 13a–d as functions of Ca for four different Re. Points correspond to the numerical results and lines to the asymptotic estimates $l \approx Ca^{-1/3}$ and $l \approx Ca^{-1/2}$. The data confirms the existence of two different regimes and verifies the above asymptotic limits. They further demonstrate that the transition from the capillary-gravity to the capillary-inertia regime is not fixed. More specifically, with increasing Re the capillary-gravity regime

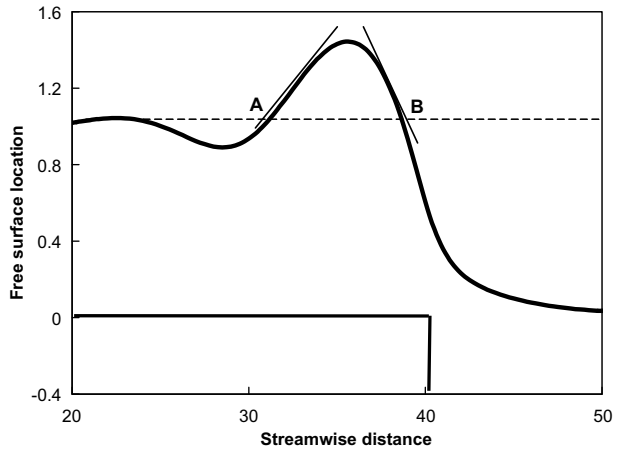

Fig. 12. The definition of the streamwise lengthscale as the segment, AB, marked on the horizontal line $y = 1$ by the tangents to the capillary ridge at the locations of maximum absolute slope.

rapidly shrinks towards the small-Ca end of the plots, in quantitative agreement with the prediction offered by Eq. (14). However, it is reasonable to suspect that the extent of the agreement down to the numerical coefficient in Eq. (14) is probably fortuitous.

The inertial scaling law, Eq. (13), may also be recovered by requiring that the capillary waves caused by the step disturbance remain stationary. In other words, the length of the capillary waves (the streamwise length scale) is such that their group velocity balances the surface velocity of the undisturbed film. (Waves travel at their group velocity, which for capillary waves is higher than their phase velocity, i.e. they propagate ahead of a moving disturbance. This explains why in the present reference frame – where the disturbance is fixed and the liquid has a free surface velocity – the capillary waves appear before the steps.)

This equivalent approach is rigorously substantiated by solving the Orr–Sommerfeld equation subject to the appropriate free surface boundary conditions. A standard spectral solver has been used (Schmid and Henningson, 2001) and the linear phase and group velocities have been computed as a function of Re, We and length of the wave. Thus, it has been confirmed that – inside the parametric

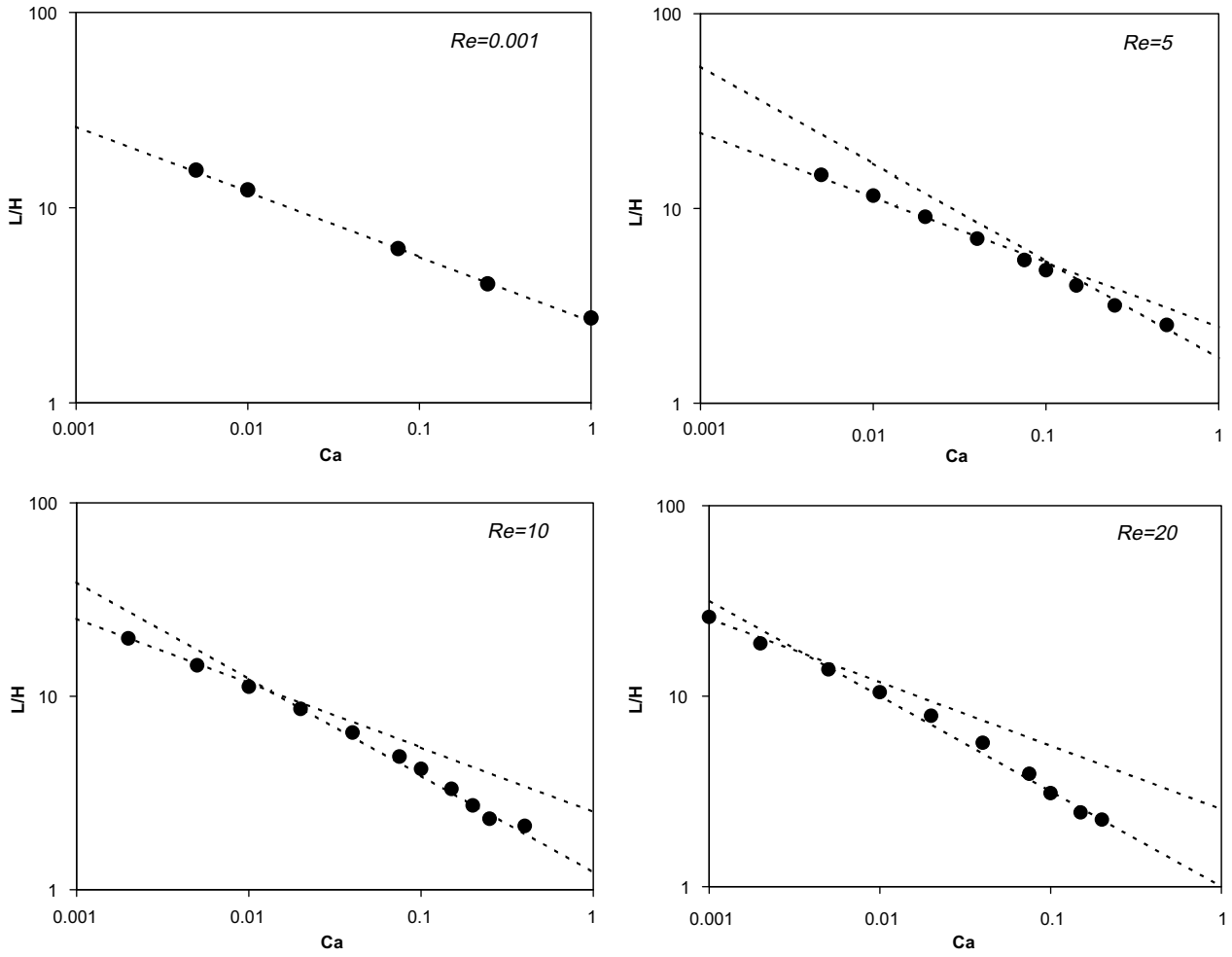

Fig. 13. The variation of the dimensionless streamwise lengthscale as a function of Ca for $Re = 0.001$, 5, 10 and 20. Points are computational data and lines are the functions $Ca^{-1/3}$ and $Ca^{-1/2}$.

region defined by Eq. (14) – the restriction to wavetrains traveling with the free surface velocity leads to wavelengths in agreement with the prediction of Eq. (13).

The above approach may be demonstrated analytically by a very simple model (albeit, of questionable accuracy). If the film flow is assumed inviscid, with a uniform velocity profile and subject only to capillary restoring forces, then the classical water wave results apply. Thus, phase and group velocities are respectively $c^2 = (\sigma k/\rho)\tanh(kH) \approx \sigma k^2 H/\rho$ and $c_g \approx 2c$, where the wavenumber $k = 2\pi/L$. By demanding that c_g be equal to the free surface velocity, $gH^2/2\nu$, the scaling of Eq. (13) is readily recovered.

4.2. The flow structure at a step-in

Two interesting effects of inertia have been observed at a step-in: (i) The decline and disappearance of the capillary waves upstream of the step. (ii) The expansion of the separation eddy that forms at the edge of the step. The results of Section 3.2 have shown that the former transition is governed by the Weber number, and therefore occurs when inertia overcome capillary effects. Also, the separation eddy has been shown to form at very small *Re*, to remain relatively restricted in size at intermediate *Re*, and then to grow continuously after the inertia-capillary transition.

Based on the above observations, we may envision the following three stages in the evolution of the flow with increasing inertia: At zero *Re*, the falling liquid does not possess momentum to bridge the gap at the step-in, and is trapped at the edge of the overhang. The curvature of the liquid bulge thus formed results in a positive capillary pressure, which provides the force to drive the liquid horizontally along the face of the step.

At low *Re*, the mechanism remains qualitatively similar as long as capillary forces dominate inertia forces: Falling liquid masses are decelerated at the edge of the step, their *x*-momentum turning predominantly into capillary potential energy. This process leads to the formation of a pinch at the edge of the step, which gives the impression that the flow is chocked (Kalliadasis et al., 2000). A convenient representation of the flow structure is provided by a contour plot of pressure. Such a plot is shown in Fig. 14a for the conditions $\delta = 1$, $Ca = 0.075$, $Re = 10$. It is evident that the capillary pressure at the free surface determines the pressure profile throughout the entire film, and a gradual drop is observed from the maximum below the capillary ridge to the minimum after the pinch, the latter being practically equal to the atmospheric pressure.

With increasing *Re*, the liquid progressively resists capillary arrest at the steep topographic change. Representative of the pressure distribution under these conditions is the contour plot of Fig. 14b, which corresponds to $\delta = 1$, $Ca = 0.075$, $Re = 50$. Here, we observe that the capillary pressure at the free surface ceases to be representative of the distribution inside the film, and a pronounced low-pressure region starts to develop downstream of the pressure singularity at the edge. Indeed, both $\partial p/\partial x$ and $\partial p/\partial y$ experience there a negative jump, as may be readily verified by the discontinuous change of terms such as $u\,\partial u/\partial x$ and $u\,\partial v/\partial x$ when moving downward along the overhanging wall and into the flow. The low-pressure eddy plays a key role in deflecting the film towards the wall and thus preventing its detachment advocated by the component of gravity normal to the inclined free surface.

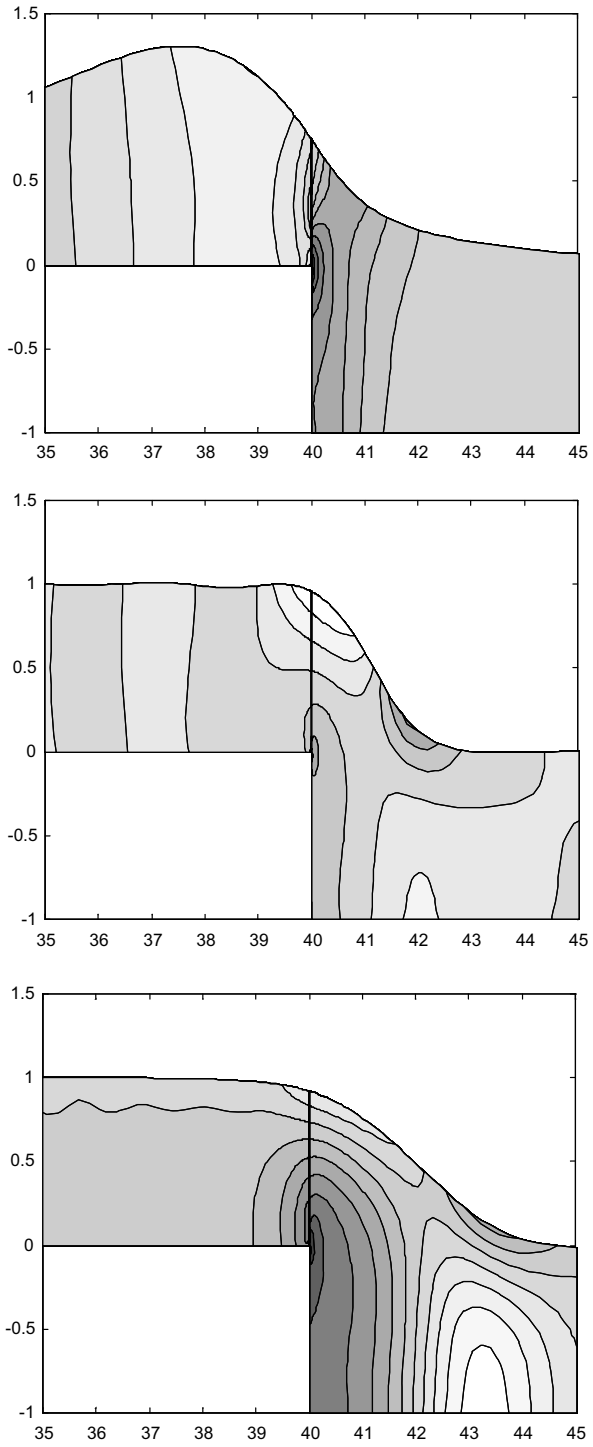

Fig. 14. The evolution with increasing *Re* of the pressure field (bright: high, dark: low) around a step-in with $\delta = 1.0$, for $Ca = 0.075$. $Re = 10$ (a), 50 (b) and 100 (c).

Finally, at high enough Re the capillary waves have totally disappeared and the film leaves the overhanging wall in the form of a free-falling sheet with minimum pressure losses at the edge. The re-attachment point of this sheet to the retracted wall moves further downstream the higher the Re. Because of the abrupt change in momentum direction that takes place there, the reattachment point appears in a pressure contour as a local maximum (Fig. 14c, for $\delta = 1$, $Ca = 0.075$, $Re = 100$).

The above steady-state analysis of the flow structure at a step-in is based on the premise that the liquid always remains attached to the wall. It is natural to expect that, for a deep enough step, the film will detach and turn into a waterfall. The convergence of our numerical scheme in the range of δ considered is taken as an indirect proof that a solution with the liquid fully attached is possible. Whether this solution is stable, and thus observable, is a different question. For example, the transition from an attached to a detached liquid clearly relates to whether air can access inside the flow, and this could occur as a result of an instability of the presently computed steady flow.

With respect to the question of stability, we draw attention to the discussion by Kalliadasis and Homsy (2001) and by Davis and Troian (2005) on the effect of recirculation below a capillary ridge on its robustness. In particular, the Stokes ridge at a step-in was shown by them to be stable, whereas a deceivingly similar capillary ridge behind a progressing contact line is unstable to transverse disturbances and breaks into fingers. The different behavior in the two flows was attributed by the latter authors to the existence of a recirculation region in the latter and its lack in the former.

4.3. The flow structure at a step-out

Apart from the evolution of the capillary features upstream of the step (which is similar to the already discussed evolution at the step-in), the main characteristic of the flow structure at a step-out is the inertial ridge. Thus, two questions arise from the results presented in Section 3.3: (i) Can we predict the conditions for the onset of the ridge? (ii) How does the structure of the flow evolve parametrically with increasing inertia?

Relative to the first question, we presume that at low/intermediate Re the inertia of the ejecting liquid is balanced mainly by surface tension (that resists deformation) and gravity (that pulls the liquid downward). Thus, at small deformation there is no significant contribution from an inertial mechanism, an assumption that seems justified in view of the postponed appearance of a separation eddy (Fig. 11). The aforementioned balance is expressed by the following order-of-magnitude equation:

$$\rho U \frac{(UH/L)}{L} \approx \sigma \frac{H}{L^3} + \rho g \Rightarrow \frac{Re}{3} \approx Ca^{-1}\left(\frac{H}{L}\right) + \left(\frac{L}{H}\right)^2, \tag{15}$$

where inertia is now in the y-direction and is represented by terms such as $u\partial v/\partial x$ or $v\partial v/\partial y$, with v scaling like (UH/L). Here, as in Eq. (12), viscous forces are included implicitly through the definition of the velocity scale, U. Thus, the term "ρg" on the r.h.s. of Eq. (15) actually represents the local imbalance between gravity and viscous forces.

The key parameter is L, the lengthscale in the streamwise direction, whose evolution at the onset of the ridge is shown in Fig. 9b. At high Ca (low surface tension), the deformation induced by the inertial jet exiting the step is predominantly determined by the width of the protruding liquid, which is roughly equal to the liquid film thickness. For $L = H$, we obtain from Eq. (15)

$$\frac{Re}{3} \approx Ca^{-1} + 1 \Rightarrow \frac{Re \cdot Ca}{1 + Ca} \approx \text{const.} \tag{16}$$

With decreasing Ca, L grows and eventually scales according to Eq. (11). This happens because the liquid exiting the step-out has initially no x-momentum, and consequently the streamwise lengthscale is determined by a balance of the remaining capillary and gravity forces. Substituting Eq. (11) into Eq. (15) leads to the prediction

$$Re\, Ca^{2/3} \approx We^{2/3} Re^{1/3} \approx \text{const.} \tag{17}$$

In Fig. 15, we replot the data of Fig. 9b about the onset conditions, as well as the above asymptotic predictions Eqs. (16) and (17), and note a very satisfactory agreement. The failure to express Eqs. (16) and (17) solely in terms of We number indicates that viscous forces have a non-trivial role on the onset of the inertial ridge, perhaps through a boundary layer effect. The 1/3 exponent of Re in Eq. (17) suggests that the main viscous effect is along the free streamline of a separated region rather than along a no-slip wall. A reasonable conjecture is that the relevant separated region is the upstream eddy at the foot of the step (see Fig. 11).

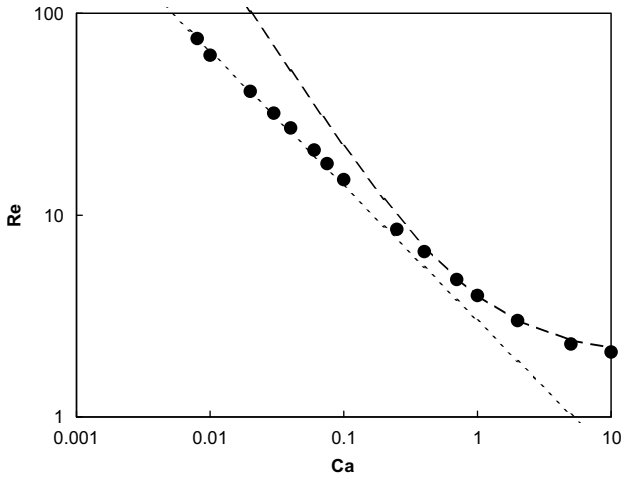

Fig. 15. Comparison between computations and asymptotic predictions, for the onset of the inertial ridge at a step-out. Dashed curve, Eq. (16); dotted line, Eq. (17).

Next, we discuss the structure of the flow using the pressure field as a diagnostic. Fig. 16 shows pressure contours with increasing Re for $Ca = 0.075$, and reveals two different mechanisms: At low inertia, the pressure distribution inside the film is dictated by the capillary features at the free surface. Thus, the negative curvature at the depression in front of the step, in combination with the positive curvature over the step, create an adverse pressure gradient that decelerates the liquid upstream of the step. Evidently, this mechanism persists up to higher Re the stronger the capillary forces.

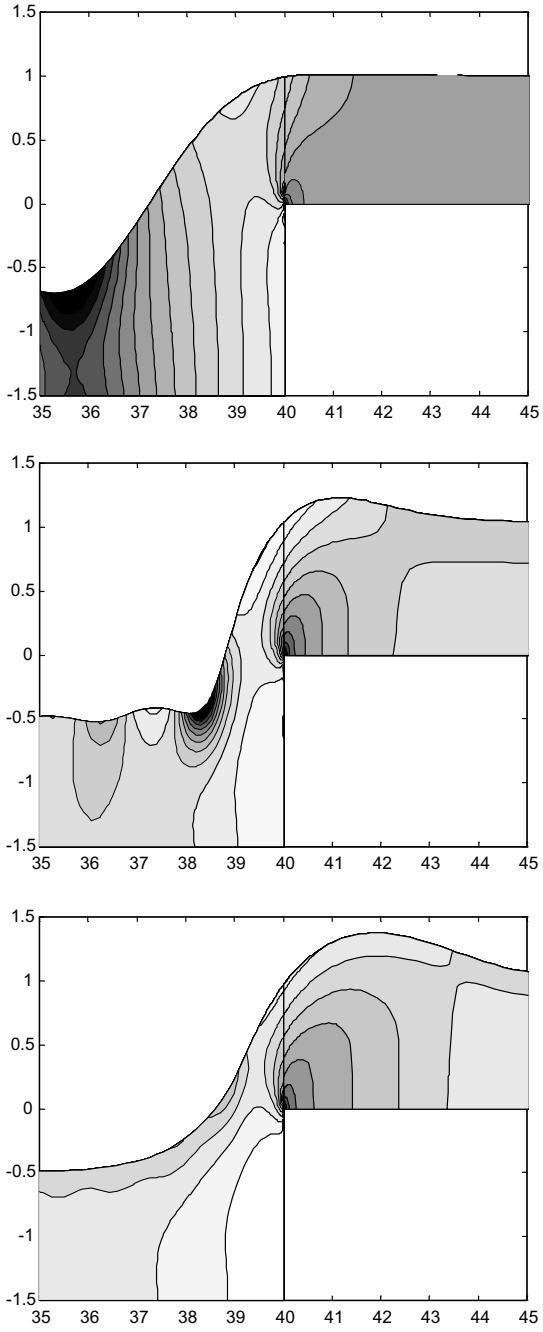

Fig. 16. The evolution with increasing Re of the pressure field (bright: high, dark: low) around a step-out with $\delta = 1.5$, for $Ca = 0.075$. $Re = 20$ (a), 60 (b) and 100 (c).

At the opposite end of high Re, inertial forces overcome capillary forces and this is indicated by the increasing stagnation pressure at the face of the step. Simultaneously, the inertial singularity at the edge creates a low-pressure region behind the step by the same mechanism discussed in conjunction with the step-in. However, because of the role of gravity (which is presently assisting the liquid to stay attached to the wall), flow separation downstream of the edge is postponed to even higher Re.

The above two mechanisms explain the parametric variation in the size of the inertial ridge, as depicted in Fig. 9a. More specifically, the low-Re behavior – where the size of the ridge varies strongly with Ca – is attributed to the capillary mechanism and the high-Re asymptote to the inertial mechanism.

Finally, we note that –similarly to the analysis of the step-in – the above steady-state analysis of the flow structure at a step-out is based on the premise that the liquid always remains attached to the wall. It is natural to expect that, for a combination of deep enough step and high enough inertia, the film will detach from the wall either permanently or temporarily. This phenomenon, which has been named the "teapot effect" (Kistler and scriven, 1994) is governed by contact-angle hysteresis a topic beyond the scope of the present work.

5. Conclusions

We have investigated numerically the parametric evolution with increasing inertia of vertical, steady film flow along isolated step-ins and step-outs. The capillary ridge before a step-in and the capillary depression before a step-out have been shown to change their streamwise lengthscale in a way that is directly predicted from an order-of-magnitude balance of gravity, capillary and inertia forces.

The computations have further indicated that the height of the capillary features first grows but then diminishes with increasing inertia. Their disappearance occurs when inertia forces dominate capillary forces, and is accompanied by a displacement of the key dynamics from upstream to downstream of the step. In particular, the change in flow direction imposed by the step is accomplished at low Re by a capillary mechanism operating before the step, and at high Re by an inertial mechanism operating after the step. The essence of the latter is a low-pressure region developing behind the step, which is triggered by the pressure singularity at the edge.

At a step-out, a new downstream free surface feature appears at high enough Re, caused by liquid overshoot in the horizontal direction. The conditions for the onset of this inertial ridge are correctly predicted by an order-of-magnitude balance of gravity, capillary and inertia forces that also takes into account the parametric variation in the streamwise lengthscale. The height of the inertial ridge is shown to be restrained by capillary forces at low Re and by inertial forces (the low-pressure region) at high Re.

Finally, we note that all the aforementioned results are derived based on the assumptions of steady flow and permanent attachment of the liquid to the wall. When multiple solutions are available, the way in which the flow is actually established will probably have a bearing on the final outcome. To this end, a complementary transient analysis might be useful (see for example Khayat et al., 2004). Also, the stability properties of the presently derived steady flows are worth investigating, in particular with respect to transverse instabilities that may corrupt the two-dimensional free surface features. This investigation will hopefully be undertaken in future work.

Acknowledgements

This work was partly supported by the General Secretariat of Research and Technology of Greece through Programme "PENED2001" and by the Ministry of Education and Religious Affairs of Greece through Programme "PYTHAGORAS II". The insightful comments of two referees, which helped resolve the delicate issue of the effect of viscous forces on the scaling, are thankfully acknowledged.

References

Aksel, N., 2000. Influence of the capillarity on a creeping flow down an inclined plane with an edge. Arch. Appl. Mech. 70, 81–90.

Davis, J.M., Troian, S.M., 2005. Generalized linear stability of noninertial coating flows over topographical features. Phys. Fluids 17, 072103.

Decre, M.J., Baret, J.-C., 2003. Gravity-driven flows of viscous liquids over two-dimensional topographies. J. Fluid Mech. 487, 147–166.

Gaskell, P.H., Jimack, P.K., Sellier, M., Thompson, H.M., Wilson, M.C.T., 2004. Gravity-driven flow of continuous thin liquid films on non-porous substrates with topography. J. Fluid Mech. 509, 253–280.

Kalliadasis, S., Chang, H.-C., 1994. Drop formation during coating of vertical fibres. J. Fluid Mech. 261, 135–168.

Kalliadasis, S., Homsy, G.M., 2001. Stability of free-surface thin-film flows over topography. J. Fluid Mech. 448, 387–410.

Kalliadasis, S., Bielarz, C., Homsy, G.M., 2000. Steady free-surface thin film flow over two-dimensional topography. Phys. Fluids 12, 1889–1898.

Khayat, R.E., Kim, K.-T., Delosquer, S., 2004. Influence of inertia, topography and gravity on transient axisymmetric thin-film flow. Int. J. Numer. Meth. Fluids 45, 391–419.

Kistler, S.F., Scriven, L.E., 1994. The teapot effect: sheet-forming flows with deflection, wetting and hysteresis. J. Fluid Mech. 263, 19–62.

Kliakhandler, I.L., Davis, S.H., Bankoff, S.G., 2001. Viscous beads on vertical fibre. J. Fluid Mech. 429, 381–390.

Malamataris, N., Vlachogiannis, M., Bontozoglou, V., 2002. Solitary waves on inclined films: flow structure and binary interactions. Phys. Fluids 14, 1082–1094.

Mazouchi, A., Homsy, G.M., 2001. Free surface Stokes flow over topography. Phys. Fluids 13, 2751–2761.

Noakes, C.J., King, J.R., Riley, D.S., 2006. On the development of rational approximations incorporating inertial effects in coating and rimming flows: a multiple-scales approach. Quart. J. Mech. Appl. Math. 59, 163–190.

Oron, A., Davis, S.H., Bankoff, S.G., 1997. Long-scale evolution of thin liquid films. Rev. Mod. Phys. 69, 931–980.

Pozrikidis, C., 1988. The flow of a liquid film along a periodic wall. J. Fluid Mech. 188, 275–300.

Prichard, W.G., Scott, R.L., Tavener, S.J., 1992. Numerical and asymptotic methods for certain viscous free-surface flows. Philos. Trans. Roy. Soc. A340, 1–14.

Roberts, A.J., Li, Z., 2006. An accurate and comprehensive model of thin fluid flows with inertia on curved substrates. J. Fluid Mech. 553, 33–73.

Ruschak, K.J., Weinstein, S.J., 2003. Laminar, gravitationally driven flow of a thin film on a curved wall. ASME J. Fluids Eng. 125, 10–17.

Schmid, P.J., Henningson, D.S., 2001. Stability and Transition in Shear Flows. Springer, Berlin.

Stillwagon, L.E., Larson, R.G., 1990. Leveling of thin films over uneven substrates during spin coating. Phys. Fluids A 2, 1937–1944.

Valluri, P., Matar, O.K., Hewitt, G.F., Mendes, M.A., 2005. Thin film flow over structured packings at moderate Reynolds numbers. Chem. Eng. Sci. 60, 1965–1975.

Webb, R.L., 1994. Principles of Enhanced Heat Transfer. Wiley, New York.